SUPPLEMENTAL MATERIALS

METHODS

MRI acquisition

All images were acquired using a 3T magnetic resonance imaging (MRI) scanner (Siemens Skyra, Siemens Medical Systems, Erlangen, Germany) using a 32-channel head coil. The MRI protocol included: a) three-dimensional magnetization prepared rapid gradient-echo T1-weighted sequence (TR=3000 ms, TE=2.47 ms, TI=1000 ms, flip angle=7 degrees, voxel size=0.8×0.8×0.8 mm^3, 224 contiguous slices); b) T2-weighted sequence (TR=8000 ms, TE=95.0 ms, voxel size=0.5×0.5×3 mm^3, 62 contiguous slices; c) T2* echo-planar imaging for resting-state functional MRI (fMRI) (TR=1000 ms, TE=35 ms, flip angle=60 degrees, voxel size=2.1×2.1×2.1 mm^3, 70 contiguous slices, 400 volumes, multiband acceleration factor=7; during the acquisition of this sequence, subjects were asked to rest with their eyes closed without falling asleep); d) twice-refocused EPI sequence for diffusion-weighted MRI (dMRI) (TR=4700 ms, TE=100 ms, flip angle=80 degrees, voxel size=1.8×1.8×2 mm^3, 78 contiguous slices, b-values=1000, 2000 s/mm^2 with 32 directions each repeated twice and 5 b=0 images also repeated twice).

Structural MRI analysis

T2-hyperintense and T1-hypointense lesion volumes were measured on the T2-weighted and T1-weighted images, using a semi-automated segmentation technique based on user-supervised local thresholding (Jim version 5; Xinapse Systems, Northants, England) (http://www.xinapse.com), and compared between multiple sclerosis (MS) patients with depression (MS-D) and without depression (MS-nD). For each patients' group, lesion probability maps were obtained using FMRIB software library (FSL 5.0, http://www.fmrib.ox.ac.uk/fsl/) (1), as previously described (2). In the resulting lesion probability map, the intensity of each voxel represents the probability of that voxel to be a

lesion in that patients' group. The probability of lesion occurrence in MS-D and MS-nD was compared with a voxel-wise non-parametric statistic as implemented in FSL's randomize, entering age and gender as covariates, with 5000 permutations. A p value <0.05, corrected for family-wise error using the threshold-free cluster enhancement (TFCE), was set.

All volumetric analyses were conducted on high-resolution T1-weighed images after correcting for the impact of white matter (WM) lesions (lesions in-painting) (3). Calculation of global brain volumes was computed in FSL's SIENAX, obtaining, for each subject, normalized brain volume (NBV), grey matter volume (GMV), and WM volume (WMV) (4). These metrics were compared between MS and HC groups, and then entered in an ANOVA between MS-D, MS-nD, and HC, followed by Bonferroni-corrected post-hoc tests. Age and gender were used as covariates in all the comparison analyses, and a corrected $p<0.05$ was set.

Processing of fMRI data

Resting-state fMRI data were preprocessed and analyzed using tools from FSL. Preprocessing was performed including: (1) slice timing correction; (2) volume realignment; (3) brain extraction; (4) regression out of linear and non-linear drift, head motion and its temporal derivative, and mean time-series from the WM and cerebrospinal fluid to control for non-neural noise (5-6); (5) non-linear alignment and normalization of anatomical and functional images with the FSL MNI152 2mm T1 standard space template; (6) spatial smoothing with a 6 mm full-width at half-maximum isotropic Gaussian kernel. The data were filtered within the standard frequency band of 0.01–0.08Hz, which is thought to reflect mainly neuronal fluctuations, and is less affected by physiological variables like respiration and aliased cardiac signals that fall in the other frequency ranges (7-11).

In addition, in order to denoise fMRI data further and to reduce motion, physiological, and other artefacts, independent component analysis (ICA)-based X-noisefier (ICA-FIX) was applied (12-13). Components obtained from the individual ICA (by using FSL MELODIC pipeline) were manually

labeled as signal or noise for 10 subjects from each group, based on spatial maps, temporal power spectrum, and their time-series (12-13). Using these classifications, the FIX classifier (a multi-level classifier which uses over 180 features capturing components' spatial and temporal characteristics) was trained and then applied to all subjects' data (using a threshold of 20), in order to classify and remove the noise components from all the data (12-13).

Finally, since head motion can affect functional connectivity (FC) estimates and can differ systematically between groups, we sought to minimize this effect in several ways (14-16). Firstly, the motion parameters from the volume realignment step were used to exclude participants using a strict threshold of translations greater than 2 mm or rotations greater than 2° in each direction. Secondly, six temporal derivatives related to head motion (on the three translational axes and three rotational axes) were estimated and used as regressors, and ICA-based denoising was performed. Moreover, motion scrubbing (or frame censoring) has been applied to our data. In particular, the FSL motion outlier tool was used to identify individual volumes that may be influenced by excessive movement (using an intensity difference metric thresholded at the 75^{th} percentile + 1.5 times the interquartile range). These volumes plus the ones immediately before and after them were excluded from the FC calculation. Finally, mean head motion was entered as covariate in all the correlation and comparison analyses.

Processing of dMRI data

Diffusion data were preprocessed and analyzed using tools from FSL. First, the b0 image of each subject was skull-stripped using the brain extraction tool. Data was then corrected for subject motion and eddy-current induced geometrical distortions, and the diffusion sensitizing gradients (bvecs) were rotated to correct for motion. Subsequently, using the FMRIB's Diffusion Toolbox (FDT), the diffusion tensor (DT) was estimated in each voxel using a linear regression and fractional anisotropy (FA) and radial diffusivity (RD) maps were derived (these metrics were estimated from b=1000 data).

Then, tract-based spatial statistics (TBSS) analysis was used to perform a voxel-wise analysis of the whole-brain DT measures (http://www.fmrib.ox.ac.uk/fsl/tbss/index.html) (1). Briefly, the individual FA images were non-linearly registered to the FMRIB58_FA standard space, provided within FSL, and averaged to create a mean FA image. The resulting mean FA image was then thinned to create a WM tract skeleton, which was thresholded at a FA=0.2 to include only WM voxels. Each subject's aligned FA data was then projected onto this skeleton and the resulting alignment-invariant representation of the central trajectory of WM pathways was used for voxel-wise statistical analysis. Similar processes were applied to RD data, by using the individual registration and projection vectors obtained in the FA non-linear registration and skeletonization stages.

Finally, we performed global anatomically constraint tractography (ACT) (17) using MRtrix (18). First, the T1 images were co-registered on dMRI using FLIRT (FSL) with boundary-based cost function (19-20). Then we computed the fiber orientation distribution functions using the multi-shell multi-tissue constrained spherical deconvolution approach (21-22) and generated 1 million streamlines using the iFOD2 tractography algorithm (23). Considering the spatial pattern of the WM alteration related to RN disconnectivity (see Results), the structural connectivity of the fornix was investigated. To extract the fornix from the global tractograms, we defined starting and ending regions of interest (ROIs) and we selected all the streamlines connecting these ROIs. As starting ROIs, we used the bilateral hippocampus recovered by FIRST on T1 images and registered on dMRI space. As ending ROI, we considered the fornix label of the ICBM-DTI-81 White-Matter Labels atlas non-linearly co-registered to each subject dMRI space using FNIRT (FSL).

CLINICAL CORRELATIONS AND ADDITIONAL CONTROL ANALYSES

Potential clinical correlations were explored. Beck's Depression Inventory, Second Edition (BDI-II) total score was entered into partial correlation analyses (with age, gender, and motion as covariates) with the MRI metrics that were found to significantly differ between groups. BDI-II total score showed a significant negative correlation with RN-BG/thalamus FC (r=-0.300; p=0.040) and no significant correlation with FA of RN-related WM (r=-0.251; p=0.119), in the MS sample.

Our findings were controlled for potential confounders.

Firstly, head motion could affect FC results, thus we further checked this issue. Head motion estimates did not significantly differ between the groups studied. Moreover, we applied motion scrubbing in our analysis. It can be noted that the number of excluded volumes during motion scrubbing did not significantly differ between groups. Importantly, RN-BG/thalamus FC remained significantly reduced in MS-D when compared to MS-nD, both with and without motion scrubbing. See **Supplemental Table 4**.

Secondly, as some of the MS patients in our sample were taking antidepressants (**Supplemental Table 1**), the significant differences in MRI metrics between MS patients with and without depressive symptomatology were controlled for this potential confounding factor. For each subject, an imipramine equivalence dosage was computed and entered into a partial correlation analysis with the relevant MRI parameters in the group of MS patients (controlling for age, gender, motion, and group status). No significant correlation was found between antidepressant dosage and RN-BG/thalamus FC (r=-0.205; p=0.171) or FA of RN-related WM (r=0.130; p=0.431). Furthermore, antidepressant dosage was used as an additional covariate (together with age, gender, and motion) in the comparison of the relevant MRI metrics between the MS groups. MS-D still showed a significant reduction of both RN-BG/thalamus FC (F=7.286; p=0.010) and FA of RN-related WM (F=6.822; p=0.013), when compared to MS-nD.

Finally, disease duration may represent an additional confounding factor. Although numerically shorter in MS patients with depressive symptomatology, disease duration did not significantly differ

between MS groups (**Supplemental Table 1**). Moreover, no significant correlation was found between disease duration and RN-BG/thalamus FC (r=-0.231; p=0.122) or FA of RN-related WM (r=-0.121; p=0.462). Finally, when disease duration was used as an additional covariate, MS-D still showed a significant reduction of both RN-BG/thalamus FC (F=10.219; p=0.003) and FA of RN-related WM (F=5.794; p=0.021), when compared to MS-nD.

LIMITATIONS

While our work has various strengths, such as a multimodal and strong a-priori approach, some limitations should be noted. The main limitation of the study is represented by sample size, which suggests interpreting carefully the results.

Moreover, assessment of depression in MS patients, also considering the retrospective nature of our work, is challenging, and a clinical scale may not be able to fully recognize the complexity of this condition, which can be influenced by several factors. However, BDI-II is a validated and standardized instrument, resulting to be effective in screening depressive symptomatology in MS patients (24). Furthermore, we considered some potential confounding factors, for instance not including patients in treatment with interferon and ruling out major psychiatric comorbidities, as well as controlling our results for antidepressant therapy. Most notably, the focus of the present work was to specifically investigate the functional and structural underpinning of depressive symptomatology emerging in MS, independently from its causal or contributing factors. Additionally, our study is cross-sectional, thus allowing only to detect potential statistical associations between different alterations.

The small size of the investigated brainstem nuclei is another limitation that needs to be taken into account. Considering this, the reported findings could be driven by a general alteration of the brainstem in a subgroup of MS patients. However, we found altered connectivity in the RN and

VTA (which both have been implicated in depression), but not in the SN (not directly implicated in depression) (25). This further supports the specificity of RN (and VTA) disconnection with the emerging depressive symptomatology in MS.

Finally, it should be noted that MS patients with depressive symptomatology were younger than those without such symptomatology. Although all our results were controlled for age, a potential effect of this factor cannot be completely excluded. Depressed MS patients, together with younger age, showed higher disability score and shorter disease duration (albeit non-significantly), as well as higher lesion load and comparable reduction of brain volume, when compared to non-depressed MS patients. This might suggest MS with depressive symptomatology to be a more aggressive condition. Considering our results (as well as the control analyses on the various potential confounding factors) depressive symptomatology is likely to emerge, rather than as an unspecific psychological reaction to a more aggressive condition, as a consequence of a specific functional-structural alteration involving neurotransmitter-related areas.

In conclusion, the results from this work pave the way to further investigations. Future studies are warranted to confirm and extend our findings, ideally by involving larger samples, including a complete and specific clinical assessment for depression (as well as a control group of patients affected by major depression), using a longitudinal perspective, and using more advanced fMRI and/or dMRI techniques, which may allow a better investigation of the complex relationship between MS and depression.

SUPPLEMENTAL FIGURES AND TABLES

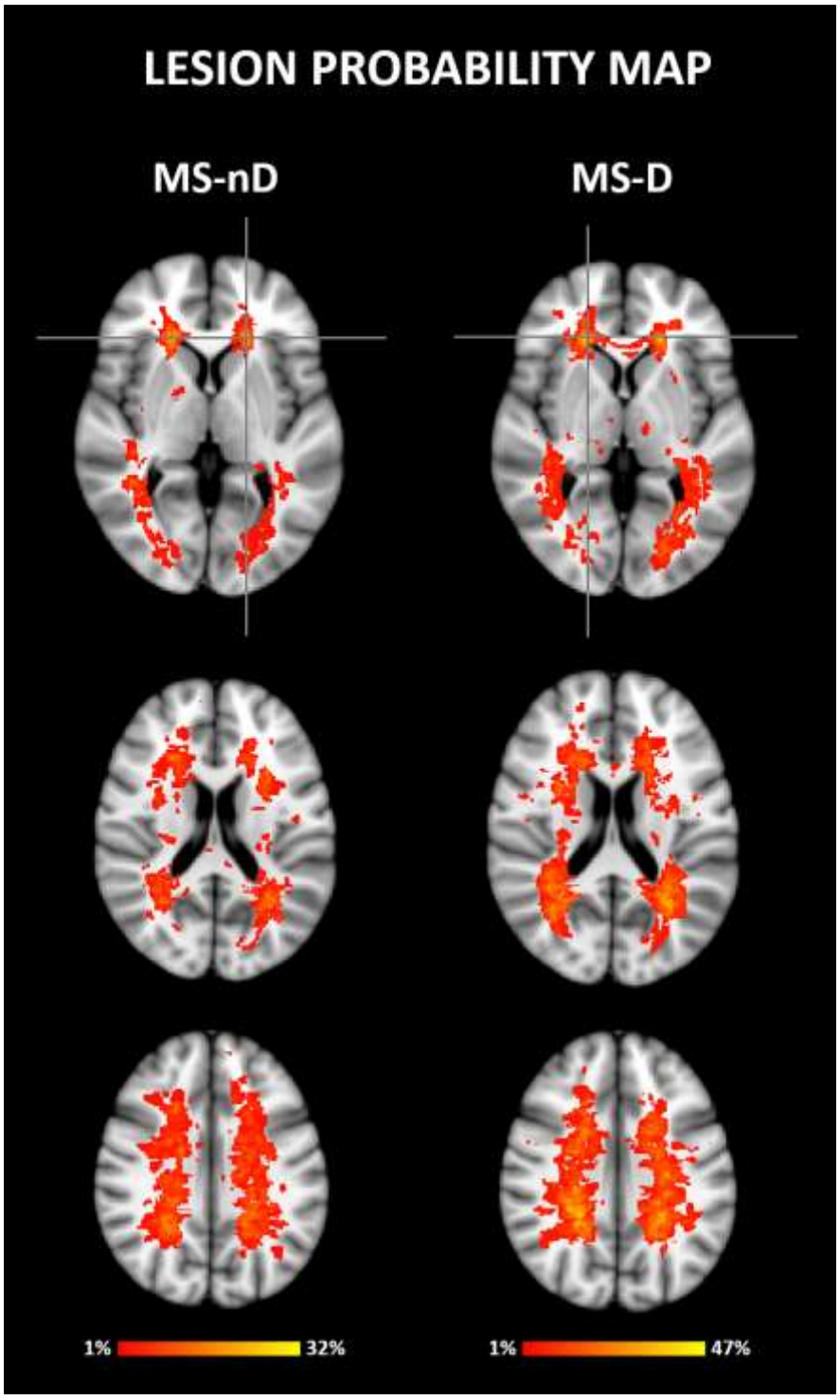

Supplemental Figure 1. Lesion probability map in MS-D and MS-nD
Lesion probability map in MS-nD and MS-D patients, overlaid on the Montreal Neurological Institute (MNI) standard brain template, showing the probability of each voxel to contain a lesion in each group. Peaks of lesion frequency is identified by crosshairs. The color scale denotes the probability range.
Abbreviations: MS-nD, multiple sclerosis without depressive symptoms (BDI<14); MS-D, multiple sclerosis with depressive symptoms (BDI≥14).

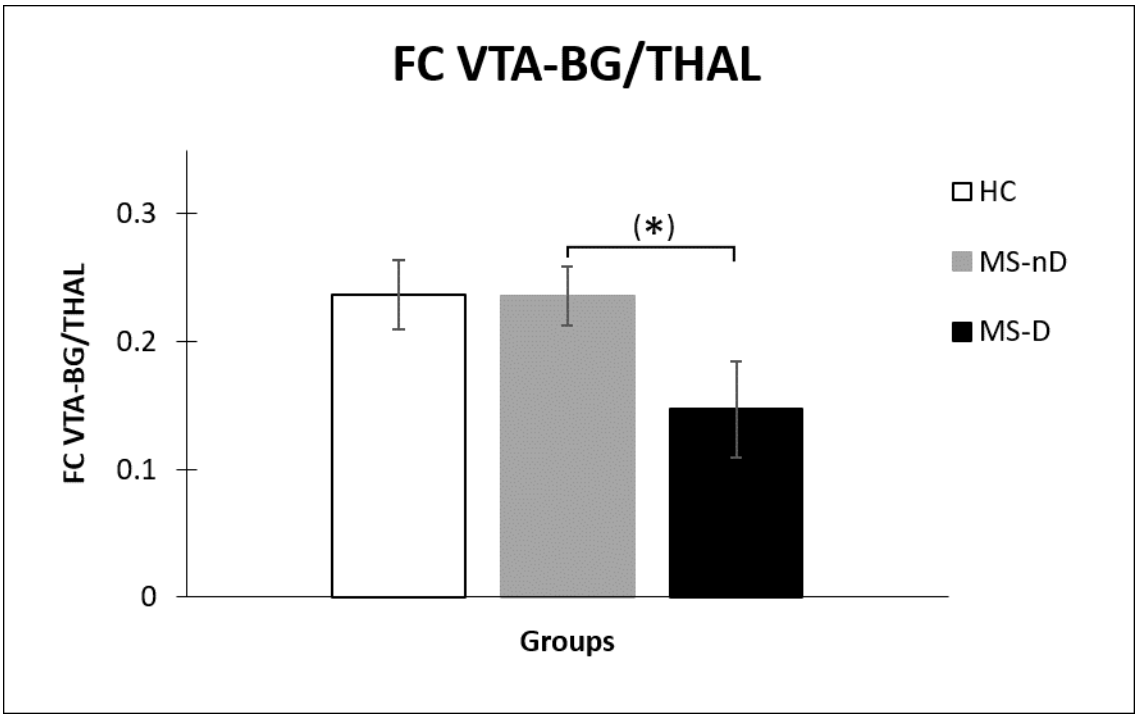

Supplemental Figure 2. FC VTA-BG/Thal in MS-D and MS-nD
Comparison of FC VTA-BG/Thal between MS-D, MS-nD, and HC (with age, gender, and motion as covariates).
(*) uncorrected $p<0.01$
Abbreviations: HC, healthy controls; MS-nD, multiple sclerosis without depressive symptoms (BDI<14); MS-D, multiple sclerosis with depressive symptoms (BDI≥14); FC, functional connectivity; VTA, ventral tegmental area; BG, basal ganglia; Thal, thalamus.

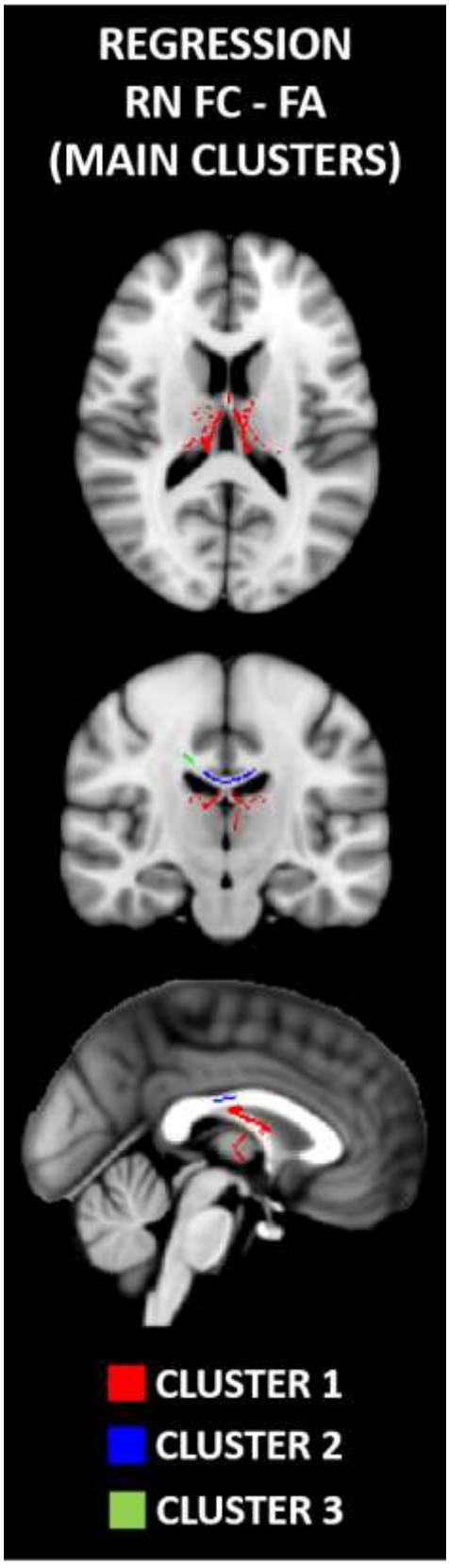

Supplemental Figure 3. Main clusters from the regression between RN-related FC and FA
The main clusters resulting from the regression analysis between RN-related FC and whole brain FA (at a TFCE-corrected p=0.05), mapped onto standard T1 Montreal Neurological Institute (MNI) template at x=0, y=-18, z=15.
Abbreviations: RN, raphe nucleus; FC, functional connectivity; FA, fractional anisotropy.

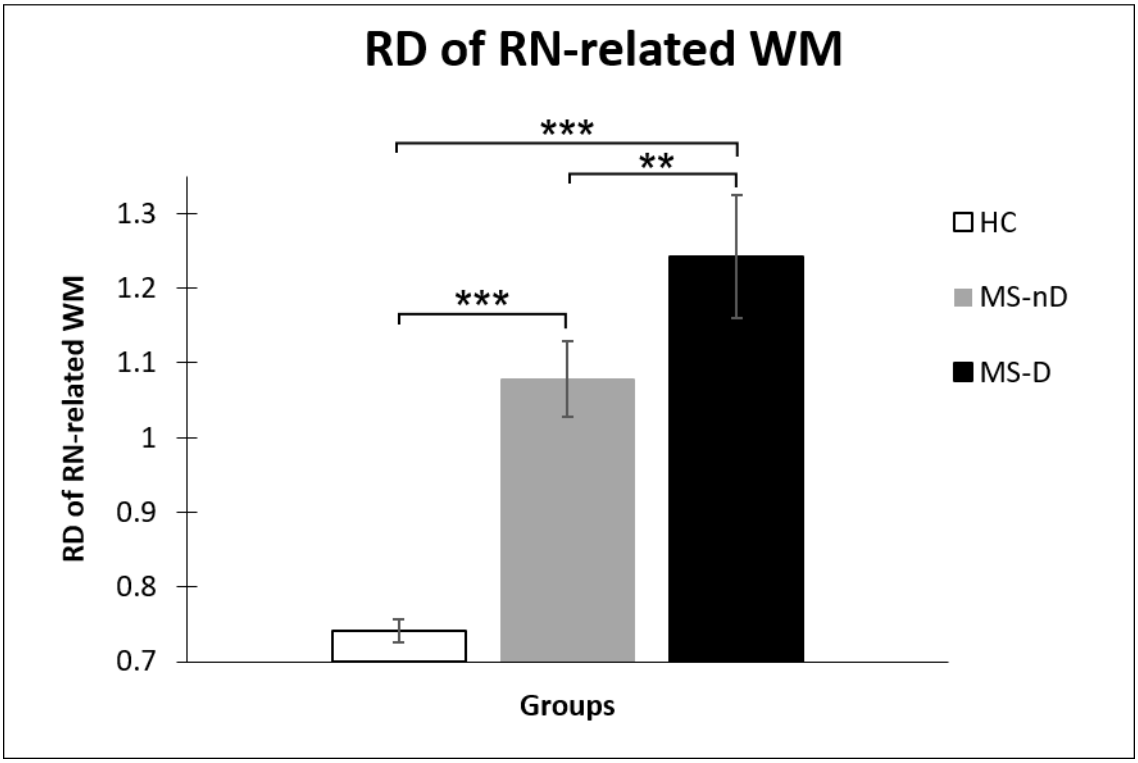

Supplemental Figure 4. RD of RN-related WM in MS-D and MS-nD
Comparison of RD in RN-related WM between MS-D, MS-nD, and HC (with age, gender, and motion as covariates).
*** $p<0.001$, ** $p<0.01$
Abbreviations: HC, healthy controls; MS-nD, multiple sclerosis without depressive symptoms (BDI<14); MS-D, multiple sclerosis with depressive symptoms (BDI≥14); RD, radial diffusivity; RN, raphe nucleus; WM, white matter.

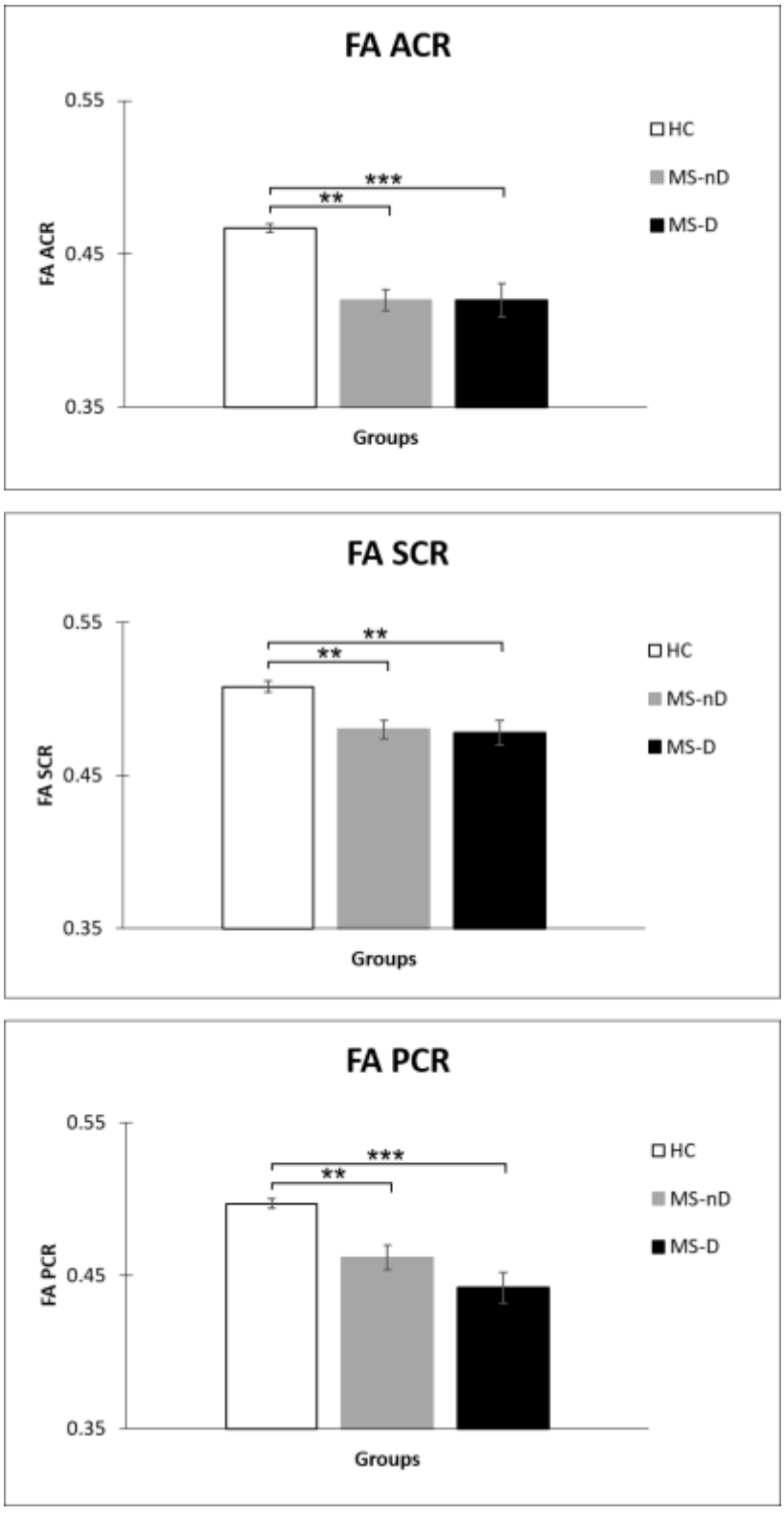

Supplemental Figure 5. FA of corona radiata in MS-D and MS-nD
Comparison of FA of ACR, SCR and PCR between MS-D, MS-nD, and HC (with age, gender, and motion as covariates).
*** $p<0.001$, ** $p<0.01$
Abbreviations: HC, healthy controls; MS-nD, multiple sclerosis without depressive symptoms (BDI<14); MS-D, multiple sclerosis with depressive symptoms (BDI≥14); FA, fractional anisotropy; ACR, anterior corona radiata; SCR, superior corona radiata; PCR, posterior corona radiata.

Supplemental Table 1. Subject Demographic and Clinical Information

	MS-nD	MS-D	HC	ANOVA	MS-D vs. HC	MS-nD vs. HC	MS-D vs. MS-nD
Sample Size n	31	19	37				
Age mean (SD)	54.8 (8.5)	45.4 (9.8)	45.9 (10.5)	F=8.740; p<0.001	p>0.99	p=0.001	p=0.004
Male/female n (%)	9/22 (29/71)	10/9 (52.6/47.4)	20/17 (54.1/45.9)	$\chi2$=4.813; p=0.090			
Disease duration (SD)	14.4 (11.8)	11.8 (8.1)					t=0.835; p=0.408
MS PP n (%)	13 (41.9)	9 (47.4)					$\chi2$=0.141; p=0.707
MS SP n (%)	12 (38.7)	6 (31.6)					$\chi2$=0.260; p=0.610
MS RR n (%)	6 (19.4)	4 (21.1)					$\chi2$=0.021; p=0.884
EDSS median (range)	4.0 (0-6)	6.0 (1-6.5)					U=203.5; p=0.124
FSS mean (SD)	4.0 (1.7)	5.0 (1.4)					U=170.5; p=0.034
BDI mean (SD)	4.9 (3.9)	17.1 (3.6)					t=11.0; p<0.001
MS therapy n (%)	20 (64.5)	14 (73.6)					
Dimethyl fumarate	4 (12.9)	2 (10.5)					
Fingolimod	2 (6.4)	0					
Glatiramer acetate	5 (16.1)	6 (31.5)					
Natalizumab	1 (3.2)	2 (10.5)					
Ocrelizumab	4 (12.9)	2 (10.5)					
Rituximab	3 (9.6)	1 (5.2)					
Siponimod	1 (3.2)	1 (5.2)					
Antidepressnts n (%)	4 (12.9)	7 (36.8)					
Bupropion	1 (3.2)	1 (5.2)					
Duloxetine	2 (6.4)	3 (15.7)					
Citalopram	1 (3.2)	1 (5.2)					
Venlafaxine	0	1 (5.2)					
Sertraline	0	1 (5.2)					

Abbreviations: MS-nD, multiple sclerosis without depressive symptoms (BDI<14); MS-D, multiple sclerosis with depressive symptoms (BDI≥14); HC, healthy controls; MS-PP, multiple sclerosis-primary progressive; MS-SP, multiple sclerosis-secondary progressive; MS-RR, multiple sclerosis-relapsing remitting; EDSS, Expanded Disability Status Scale; BDI-II, Beck's Depression Inventory, Second Edition.

Supplemental Table 2. Brain and lesion volumes

Mean brain and lesion volumes in patients and controls

VOLUMES	**MS-D**	**MS-nD**	**HC**
(ml)	*mean (SD)*	*mean (SD)*	*mean (SD)*
NBV	1419.775 (74.557)	1409.496 (98.081)	1507.566 (86.291)
GMV	756.641 (48.685)	752.873 (59.557)	799.762 (59.945)
WMV	663.134 (42.345)	656.621 (50.099)	702.772 (48.265)
T2 LV	12.226 (10.669)	3.797 (4.182)	
T1 LV	9.360 (8.925)	2.851 (3.264)	

Comparison of mean brain and lesion volumes between patients and controls

VOLUMES	**T-TEST (MS vs. HC)**	**ANOVA**	**MS-D vs. HC**	**MS-nD vs. HC**	**MS-D vs. MS-nD**
(ml)	*F (p)*	*F (p)*	*(p)*	*(p)*	*(p)*
NBV	MS<HC 20.196 (<0.001)	9.977 (<0.001)	MS-D<HC (0.002)	MS-nD<HC (0.001)	(>0.99)
GMV	MS<HC 10.086 (0.002)	5.194 (0.008)	MS-D<HC (0.015)	MS-nD<HC (0.064)	(>0.99)
WMV	MS<HC 16.822 (<0.001)	8.529 (<0.001)	MS-D<HC (0.014)	MS-nD<HC (0.001)	(>0.99)
T2 LV					MS-D>MS-nD F=15.785 (<0.001)
T1 LV					MS-D>MS-nD F=11.967 (0.001)

Mean values of brain and lesion volumes, as well as T-tests and ANOVAs with Bonferroni-corrected post hoc tests (with age and gender as covariates) showing differences in brain and lesion volumes between groups (corrected $p<0.05$).

Abbreviations: NBV, normalized brain volume; GMV, grey matter volume; WMV, white matter volume; T2 LV, mean T2-hyperintense lesion volume; T1 LV, mean T1-hypointense lesion volume; MS, multiple sclerosis; MS-nD, multiple sclerosis without depressive symptoms (BDI<14); MS-D, multiple sclerosis with depressive symptoms (BDI≥14); HC, healthy controls.

Supplemental Table 3. WM subclusters from the regression between RN-related FC and FA

Subclusters	Anatomical Regions	CS	peak (x, y, z)	corrected p
1	WM encompassing thalamic/basal ganglia areas, including the fornix	1515	-10, -28, 13	0.002
2	body of corpus callosum	322	3,-18, 24	0.0038
3	body of corpus callosum/superior corona radiata right	216	18, -23, 34	0.042

Main WM subclusters resulting from the regression analysis between RN-related FC and whole brain FA, at a TFCE-corrected p=0.05 (with cluster size > 100).
Abbreviations: WM, white matter; RN, raphe nucleus; FC, functional connectivity; FA, fractional anisotropy; CS, cluster size.

Supplemental Table 4. Control analyses for head motion

	MS-D	**MS-nD**	**HC**	
	mean (SD)	*mean (SD)*	*mean (SD)*	
Head Motion	0.26 (0.17)	0.30 (0.14)	0.21 (0.11)	
Number of excluded frames	18.84 (19.14)	19.74 (14.25)	15.59 (14.17)	
	ANOVA	**MS-D vs. HC**	**MS-nD vs. HC**	**MS-D vs. MS-nD**
	F (p)	*(uncorr. p)*	*(uncorr. p)*	*(uncorr. p)*
Head Motion	1.402 (0.252)	(0.184)	(0.161)	(0.995)
Number of excluded frames	1.105 (0.336)	(0.441)	(0.148)	(0.586)
	ANOVA	**MS-D vs. HC**	**MS-nD vs. HC**	**MS-D vs. MS-nD**
	F (p)	*(p)*	*(p)*	*(p)*
FC RN-BG/Thal (without motion scrubbing)	7.123 (0.001)	MS-D<HC (0.002)	(>0.99)	MS-D<MS-nD (0.006)

Mean values of head motion and number of excluded frames during motion scrubbing, as well as ANOVAs with post hoc tests (with age and gender as covariates) showing no differences between groups in these parameters (uncorrected p is reported). ANOVAs with Bonferroni-corrected post hoc tests (with age, gender, and motion as covariates) showing differences between groups in RN-related FC without motion scrubbing (corrected $p<0.05$).

Abbreviations: FC, functional connectivity; RN, raphe nucleus; BG, basal ganglia; Thal, thalamus; MS-nD, multiple sclerosis without depressive symptoms (BDI<14); MS-D, multiple sclerosis with depressive symptoms (BDI≥14); HC, healthy controls.

REFERENCES

1. Woolrich MW, Jbabdi S, Patenaude B, Chappell M, Makni S, Behrens T, et al. Bayesian analysis of neuroimaging data in FSL. Neuroimage. 2009 Mar;45(1 Suppl):S173-86.
2. Rossi F, Giorgio A, Battaglini M, Stromillo ML, Portaccio E, Goretti B, et al. Relevance of brain lesion location to cognition in relapsing multiple sclerosis. PloS one. 2012;7(11):e44826.
3. Battaglini M, Jenkinson M, De Stefano N. Evaluating and reducing the impact of white matter lesions on brain volume measurements. Human brain mapping. 2012 Sep;33(9):2062-71.
4. Smith SM, Zhang Y, Jenkinson M, Chen J, Matthews PM, Federico A, et al. Accurate, robust, and automated longitudinal and cross-sectional brain change analysis. NeuroImage. 2002 Sep;17(1):479-89.
5. Fox MD, Snyder AZ, Vincent JL, Corbetta M, Van Essen DC, Raichle ME. The human brain is intrinsically organized into dynamic, anticorrelated functional networks. Proc Natl Acad Sci U S A. 2005 Jul 5;102(27):9673-8.
6. Saad ZS, Gotts SJ, Murphy K, Chen G, Jo HJ, Martin A, et al. Trouble at rest: how correlation patterns and group differences become distorted after global signal regression. Brain Connect. 2012;2(1):25-32.
7. Biswal B, Yetkin FZ, Haughton VM, Hyde JS. Functional connectivity in the motor cortex of resting human brain using echo-planar MRI. Magn Reson Med. 1995 Oct;34(4):537-41.
8. Fox MD, Raichle ME. Spontaneous fluctuations in brain activity observed with functional magnetic resonance imaging. Nat Rev Neurosci. 2007 Sep;8(9):700-11.
9. Zhang D, Raichle ME. Disease and the brain's dark energy. Nat Rev Neurol. 2010 Jan;6(1):15-28.
10. Zuo XN, Di Martino A, Kelly C, Shehzad ZE, Gee DG, Klein DF, et al. The oscillating brain: complex and reliable. Neuroimage. 2010 Jan 15;49(2):1432-45.
11. Cordes D, Haughton VM, Arfanakis K, Carew JD, Turski PA, Moritz CH, et al. Frequencies contributing to functional connectivity in the cerebral cortex in "resting-state" data. AJNR Am J Neuroradiol. 2001 Aug;22(7):1326-33.
12. Salimi-Khorshidi G, Douaud G, Beckmann CF, Glasser MF, Griffanti L, Smith SM. Automatic denoising of functional MRI data: combining independent component analysis and hierarchical fusion of classifiers. Neuroimage. 2014 Apr 15;90:449-68.
13. Griffanti L, Salimi-Khorshidi G, Beckmann CF, Auerbach EJ, Douaud G, Sexton CE, et al. ICA-based artefact removal and accelerated fMRI acquisition for improved resting state network imaging. Neuroimage. 2014 Jul 15;95:232-47.
14. Power JD, Schlaggar BL, Petersen SE. Recent progress and outstanding issues in motion correction in resting state fMRI. Neuroimage. 2015 Jan 15;105:536-51.
15. Power JD, Barnes KA, Snyder AZ, Schlaggar BL, Petersen SE. Spurious but systematic correlations in functional connectivity MRI networks arise from subject motion. Neuroimage. 2012 Feb 1;59(3):2142-54.
16. Siegel JS, Mitra A, Laumann TO, Seitzman BA, Raichle M, Corbetta M, et al. Data Quality Influences Observed Links Between Functional Connectivity and Behavior. Cereb Cortex. 2017 Sep 1;27(9):4492-502.
17. Smith RE, Tournier JD, Calamante F, Connelly A. Anatomically-constrained tractography: improved diffusion MRI streamlines tractography through effective use of anatomical information. Neuroimage. 2012 Sep;62(3):1924-38.
18. Tournier JD, Smith R, Raffelt D, Tabbara R, Dhollander T, Pietsch M, et al. MRtrix3: A fast, flexible and open software framework for medical image processing and visualisation. Neuroimage. 2019 Nov 15;202:116137.
19. Jenkinson M, Bannister P, Brady M, Smith S. Improved optimization for the robust and accurate linear registration and motion correction of brain images. Neuroimage. 2002 Oct;17(2):825-41.
20. Greve DN, Fischl B. Accurate and robust brain image alignment using boundary-based registration. Neuroimage. 2009 Oct 15;48(1):63-72.
21. Tournier JD, Calamante F, Connelly A. Robust determination of the fibre orientation distribution in diffusion MRI: non-negativity constrained super-resolved spherical deconvolution. Neuroimage. 2007 May 1;35(4):1459-72.

22. Tournier JD, Calamante F, Connelly A. Determination of the appropriate b value and number of gradient directions for high-angular-resolution diffusion-weighted imaging. NMR Biomed. 2013 Dec;26(12):1775-86.
23. Tournier JD, Calamante F, Connelly A. Improved probabilistic streamlines tractography by 2nd order integration over fibre orientation distributions. Proceedings of the International Society for Magnetic Resonance in Medicine. 2010.
24. Turner AP, Alschuler KN, Hughes AJ, Beier M, Haselkorn JK, Sloan AP, et al. Mental Health Comorbidity in MS: Depression, Anxiety, and Bipolar Disorder. Current neurology and neuroscience reports. 2016 Dec;16(12):106.
25. Anand A, Jones SE, Lowe M, Karne H, Koirala P. Resting State Functional Connectivity of Dorsal Raphe Nucleus and Ventral Tegmental Area in Medication-Free Young Adults With Major Depression. Frontiers in psychiatry. 2018;9:765.